Journal of
Synchrotron Radiation

ISSN 0909-0495

Received 22 February 2007
Accepted 13 September 2007

Structural properties of 'naked' gold nanoparticles formed by synchrotron X-ray irradiation

Chang-Hai Wang,[a] Chia-Chi Chien,[a,b] Yen-Lu Yu,[a,c] Chi-Jen Liu,[a] Cheng-Feng Lee,[a] Chih-Hsiung Chen,[a] Y. Hwu,[a,b,d,e]* Chung-Shi Yang,[f] Jung-Ho Je[g] and G. Margaritondo[h]

[a]Institute of Physics, Academia Sinica, Nankang, Taipei, Taiwan, [b]Department of Engineering and System Science, National Tsing Hua University, Hsinchu, Taiwan, [c]Department of Chemical Engineering, National Taiwan University, Taipei, Taiwan, [d]Institute of Opto-Electronics Sciences, National Taiwan Ocean University, Keelung, Taiwan, [e]National Synchrotron Radiation Research Center, Hsinchu, Taiwan, [f]Nanomedicine Research Center, National Health Research Institute, Chunan, Taiwan, [g]X-ray Imaging Center, Pohang Univeristy of Science and Technology, Pohang, Korea, and [h]Ecole Polytechnique Fédérale de Lausanne (EPFL), CH-1015 Lausanne, Switzerland. E-mail: phhwu@sinica.edu.tw

The formation of colloidal unmodified ('naked') gold nanoparticles is investigated by irradiation of a precursor solution with X-rays from a synchrotron source. An interesting morphological evolution as a function of exposure time, from cross-linked network-like structure to individual particles, has been discovered. The particle size decreased with the exposure time and was influenced by the ionic strength of the precursor solution. Contrary to γ-ray exposure, an OH radical scavenger was not required for cluster formation.

Keywords: structure; morphology; gold nanoparticles.

1. Introduction

Potential applications including biosensor (Chah *et al.*, 2005; Siwy *et al.*, 2005), bio-imaging (Lee, Oldenburg *et al.*, 2003; Osawa *et al.*, 2005; Loo, Hirsch *et al.*, 2005), tumor treatment (Sun *et al.*, 2004; Loo, Lowery *et al.*, 2005) and many others stimulate the interest in colloidal gold particles. Their fabrication and properties have been intensively investigated (Daniel & Astruc, 2004; Schmid & Corain, 2003; Glomm, 2005) with specific emphasis on possible use in cancer therapy (O'Neal *et al.*, 2004; Zharov *et al.*, 2005).

Practical applications often require a good control of the nanoparticle size, morphology, colloidal stability and specificity, which constitutes a serious challenge in materials science. To meet this challenge, chemical reduction methods are most often used. Radiolytic approaches have also been extensively explored since the 1960s (Fujita *et al.*, 1962) and the corresponding reactions were systematically studied (Belloni *et al.*, 1998; Gachard *et al.*, 1998). Photon-stimulated processes indeed offer several advantages: no need for the preliminary use of reducing agents, well characterized reaction parameters and the production of highly reduced pure nanoparticles.

The radiolytic preparation of metal particles was recently extended to X-rays (Rosenberg *et al.*, 1998; Ma *et al.*, 2000; Lee, Je *et al.*, 2003; Borse *et al.*, 2004). Karadas *et al.* (2005) analyzed the precipitation of Au nanoparticles from tetrachloriauric acid induced by a conventional X-ray source in terms of the reduction dynamics. Owing to the low reaction rate, exposure times in excess of 30 h were required.

We recently developed a new and more rapid method using X-rays from a synchrotron source to prepare well dispersed Au particles in aqueous solutions (Yang *et al.*, 2006; Wang *et al.*, 2007). This X-ray-based approach compares favorably with γ-ray irradiation. Reducing agents are created by the solvent radiolysis, but for γ-ray exposure stabilizing agents are still needed to prevent coalescence and obtain dispersed metal clusters. On the contrary, no pre-added stabilizer is required for our method.

The investigations conducted so far explored the role of the pH value and of the exposure conditions as well as the biocompatibility of the final products. The present study deals with the structure and morphology of the X-ray-produced Au nanoparticles. We analyzed the effects of the exposure time, of the ionic strength and of radical scavengers, and discovered interesting phenomena that are discussed in terms of X-ray-induced synthesis.

2. Experimental

2.1. Materials and methods

All the chemicals were of reagent grade and were used without additional purification. The gold precursor was hydrogen tetrachloroaurate trihydrate ($HAuCl_4{\cdot}3H_2O$) from

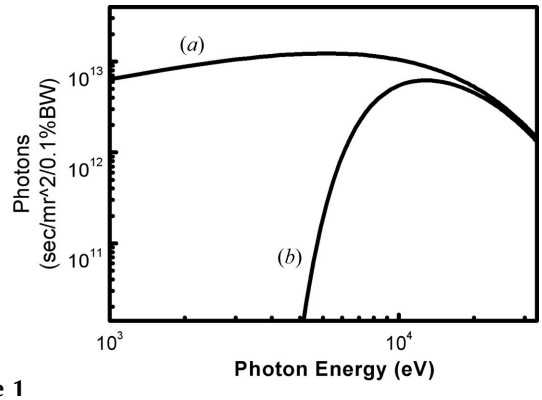

Figure 1
Photon flux as a function of the photon energy for the synchrotron white X-rays at beamline BL01A of NSRRC. (*a*) Emission from the superconducting bending magnet; (*b*) flux at the specimen position after the effects of the air and window absorption.

Aldrich (USA). The precursor solution was prepared by adding NaOH to a $HAuCl_4{\cdot}3H_2O$ solution to obtain a pH value of >9, stirring for 10 min and then waiting for 5 min to homogenize and equilibrate. For the tests on the effect of the ionic strength, different concentrations of NaCl were included in the precursor solution.

Then 10 ml of the solution was exposed to hard X-rays from the BL01A beamline of NSRRC (National Synchrotron Radiation Research Center, Hsinchu, Taiwan), whose emission spectrum estimated at the exit of the wavelength shifter insertion device is shown as curve (*a*) in Fig. 1 (Center of X-ray Optics, Lawrence Berkeley National Laboratory, http://henke.lbl.gov/optical_constants/bend2.html). The curve (*b*) in Fig. 1 shows the estimated photon energy distribution at the exposure position taking into account absorption by the windows, the air and the walls of solution-containing tubs. A slit was used to obtain a transversal beam section of 13 mm × 9 mm matching the dimensions of the tubes. Some of the studies were performed at beamline 7B2 of PLS (Pohang Light Source, Pohang, Korea) that has similar emission properties (Baik *et al.*, 2004). We used unmonochromatized ('white') X-ray beams with no optical elements except beryllium and Kapton windows. The calculated flux absorbed by the precursor solutions was centered at around 12.5 keV and was over 1×10^{12} photons s^{-1} (0.1% bandwidth)$^{-1}$ in the energy range 6.5–30 keV. The exposure time ranged from 0.5 min to 15 min.

2.2. Instrumentation and characterization

Ultraviolet-visible (UV-VIS) absorption spectra were recorded using a GBC UV/VIS 916 spectrophotometer. The surface charge for the gold nanoparticle dispersions was measured using a Malvern Zetasizer 3000 system. X-ray diffraction (XRD) measurements were performed using the synchrotron X-rays of the wiggler beamline BL17A at NSRRC, whose wavelength equals 0.1333 nm. The results were interpreted using JCPDS indexing after correction for the different X-ray source (Cu *K*, 1.5418 Å). The samples for XRD were prepared by drying concentrated colloidal solution drops overnight in a pumped desiccator. The nanocrystal size was estimated from the broadening of diffraction peaks using Scherrer's formula with a *K* value of 0.9.

The particle morphology, structure and size were measured using a Jeol JEM 2010 F field emission gun transmission electron microscope (TEM) operating at 200 kV. The samples for TEM measurements were prepared by placing droplets of nanoparticle-containing solution on carbon-coated Cu grids and allowing them to dry.

3. Results

3.1. Structural analysis

TEM and XRD results for colloidal gold particles obtained after a 5 min X-ray exposure are shown in Figs. 2 and 3. We see in Fig. 2(*a*) spherical nanoparticles, with a diameter of 20 ± 5 nm and good dispersion. The high-resolution TEM image of Fig. 2(*b*) shows the multi-domain structure that is often present in the Au nanoparticles produced by synchrotron X-ray irradiation. It has been reported that, with heating and electron beam irradiation, neighboring metallic nanoparticles can coalesce to form larger particles (Sutter *et al.*, 2005). As discussed below, Fig. 2(*b*) suggests that the imaged particle is the product of a similar coalescence mechanism involving smaller single-crystal particles.

The XRD pattern of Fig. 3 exhibits the characteristic diffraction peaks from the face-centered-cubic Au crystal planes of (111), (200), (220), (311) and (222). The average nanoparticle size was also derived from the broadening of the reflection peaks (111) and (222), obtaining 20.7 nm and 18.3 nm, consistent with TEM results.

3.2. Effects of the exposure time

Fig. 4 shows TEM images of colloidal Au nanoparticles for different X-ray exposure times. We see an interesting growth mechanism: (*a*) after 30 s of irradiation, the nanoparticles are clustered in cross-linked structures whose overall size is on the micrometer scale; (*b*) after 1 min, the interconnections between neighboring nanoparticles are modified, and almost spherical 3–5 nm particles are formed; (*c*) 5 min of irradiation fragments the overall structure producing separated particles; (*d*) for a longer irradiation, the dispersion improves and the average particle size decreases. We also found that colloidal Au nanoparticle solutions are not stable for shorter (<10 s) irradiation times and precipitate within a few minutes; longer exposures result in colloidal stability. Zeta potential measurement of colloidal gold with 5 min X-ray exposure yielded a negative value of −57.8 ± 5 mV indicating that the colloidal particles were stabilized by electrostatic repulsion.

Fig. 5 shows visible-light absorption spectra of the colloidal solution after different irradiation times, with two characteristic features: the surface plasmon resonance peak at 537–521 nm and a second peak at longer wavelengths. For 30 s of exposure, the plasmon peak is visible but weak indicating the formation of a small number of Au nanoparticles; the position (537 nm) is shifted with respect to that (520 nm) of Au

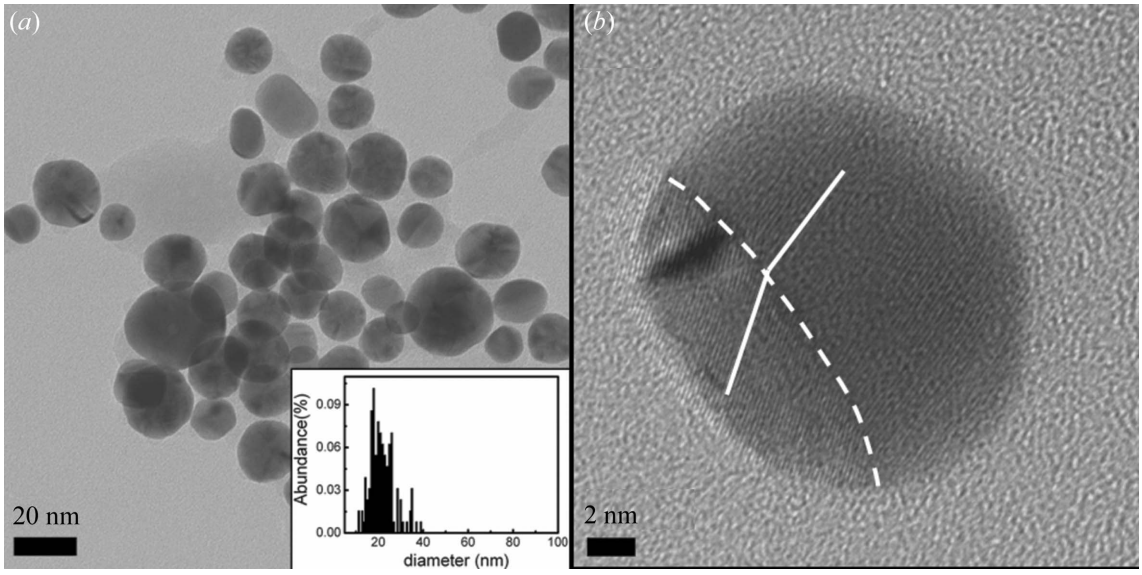

Figure 2
TEM (*a*) and high-resolution TEM (*b*) micrographs of gold nanoparticles produced by a 5 min synchrotron X-ray exposure for 10 ml precursor solution ([$HAuCl_4$] = 1 m*M*). The inset in (*a*) is the size distribution histogram of the particles. The white lines in (*b*) are a guide to the eye for the boundaries between different crystalline domains.

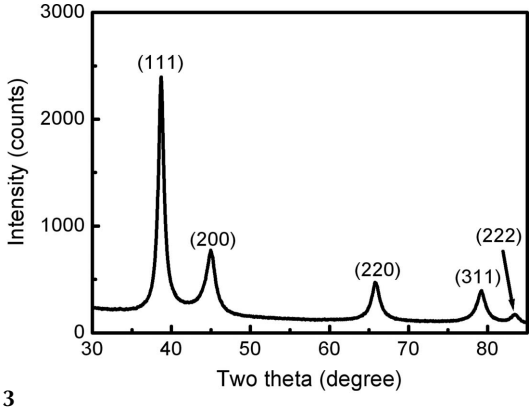

Figure 3
X-ray diffraction pattern of the colloidal gold particles as shown in Fig. 2. These results were used to derive the average particle size.

nanoparticles of comparable size (Mulvaney, 2001; Kreibig & Genzel, 1985). Together with the presence of the larger-wavelength peak, this shift suggests the existence of interconnected nanoparticles (or of precipitation).

After 1 min of exposure, the plasmon peak (now at 533 nm) is stronger and the longer-wavelength feature is weaker, suggesting that more nanoparticles are formed whereas the agglomeration decreases. After 5 min the plasmon peak practically reaches the aforementioned standard position and the second feature tends to disappear, indicating well distributed Au particles. For a longer exposure of 15 min, the plasmon peak remains almost unchanged whereas the long-wavelength feature exhibits a limited decrease.

Fig. 6 shows the effects of long-time irradiation. The sample here was first formed with 5 min irradiation and then continuously exposed to synchrotron X-rays for 7 h. The TEM image of Fig. 6 shows a tendency of the particle size to decrease to <10 nm, even though a few large particles (15–20 nm) remain. The particles are interconnected and less electron-dense than in Fig. 4(*c*). Some particles are fused together forming larger irregular shapes or producing dumb-bell-like configurations (highlighted by arrows in Fig. 6*a*). The visible-light spectrum of Fig. 6(*b*) does not reveal any change with respect to the 5 min irradiation spectrum of Fig. 5.

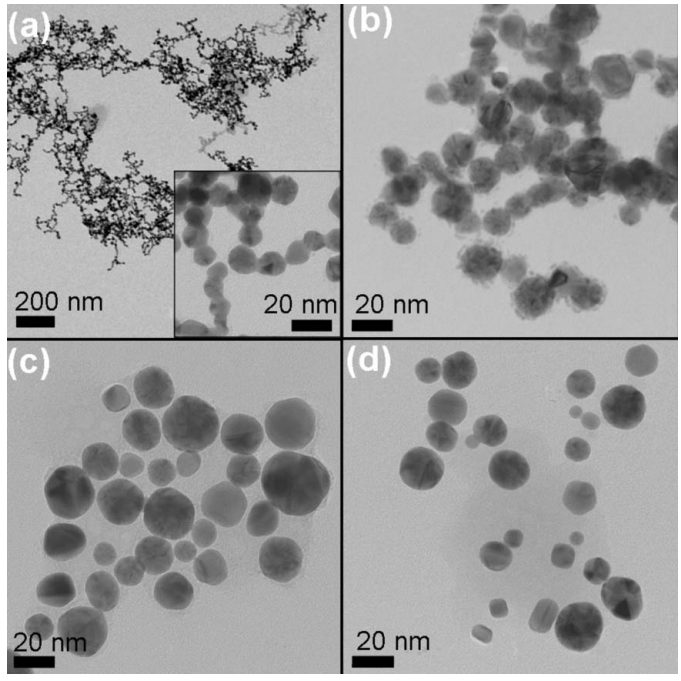

Figure 4
TEM micrographs of colloidal gold particles produced by different X-ray exposure times: (*a*) 30 s; (*b*) 1 min; (*c*) 5 min and (*d*) 15 min for 10 ml precursor solution ([$HAuCl_4$] = 1 m*M*). These results reveal a complex series of phenomena as discussed in the text, and in particular the size changes as a function of exposure.

3.3. Effect of the ionic strength

Solution conditions such as the pH value and the ionic strength can influence the morphology and stability of colloidal particles. As already mentioned, to investigate the effects of the ionic strength in our case, NaCl aqueous solutions of different concentrations were used as the solvent for the gold precursor solution.

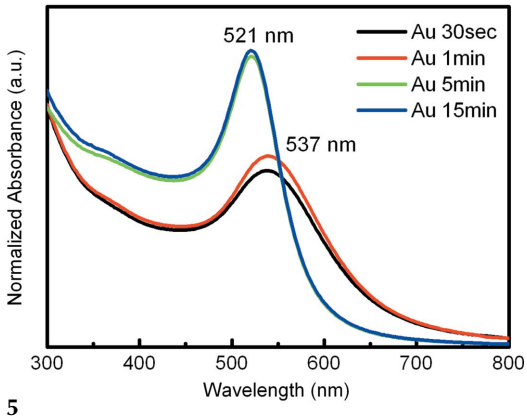

Figure 5
Visible-light absorption spectra of colloidal gold particles produced by different X-ray exposure times (30 s, 1 min, 5 min, 15 min) for a 10 ml precursor solution ($[HAuCl_4]$ = 1 m*M*). Note the dramatic change between 1 and 5 min exposure.

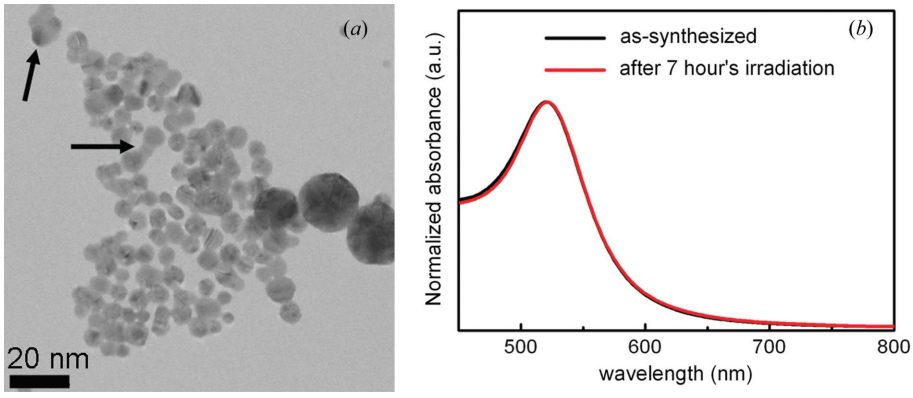

Figure 6
TEM micrograph (*a*) and visible-light absorption spectrum (*b*) of colloidal gold solutions after a long exposure (7 h) to synchrotron X-rays for a 10 ml precursor solution ($[HAuCl_4]$ = 1 m*M*). Note that no significant changes occur with respect to exposures of a few minutes.

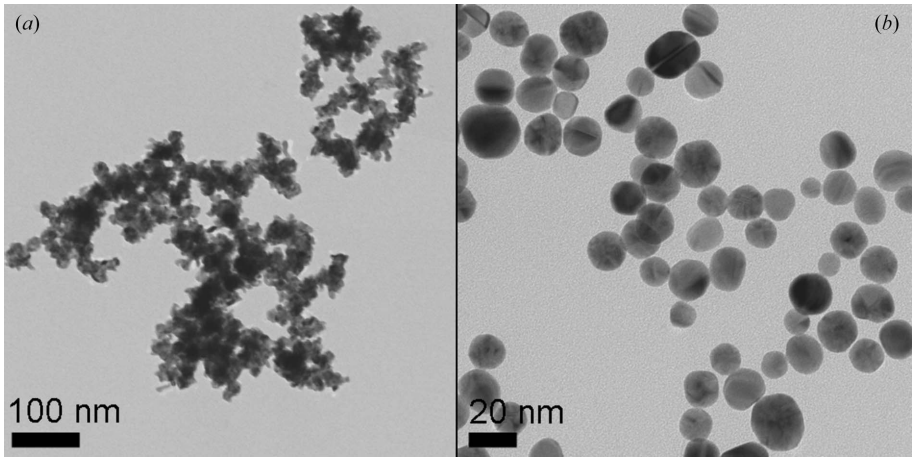

Figure 7
TEM images of gold nanoparticles formed by X-ray exposure after replacing de-ionized H_2O with a 0.01 *M* NaCl solution: (*a*) 30 s; (*b*) 10 min for a 10 ml precursor solution ($[HAuCl_4]$ = 1 m*M*). These results reveal the effects of a stronger ionic strength of the solution.

Fig. 7 shows TEM images of Au nanoparticles for a 0.01 *M* NaCl solution. Nanoparticles formed by a 30 s irradiation exhibit agglomeration and a tendency to precipitate right after the end of the exposure. A 10 min irradiation results in stable particles as shown in Fig. 7(*b*). The size is smaller (15–20 nm) and the dispersion better than for the deionized-water solution.

When the ionic strength is further increased by using 0.1 *M* and 0.5 *M* NaCl solutions, stable colloidal particles are not formed and agglomeration and precipitation occur. These results suggest that Cl^- ions might interact with the Au surface during the particle formation. These findings agree with previous studies and are reasonable in view of the particle surface chemistry (Bae *et al.*, 2002; Sylvestre *et al.*, 2004).

3.4. Tests with 2-propanol as a radical scavenger

In the photosynthesis of metal colloids by γ-ray irradiation, 2-propanol is usually added as an OH radical scavenger to prevent particles oxidation. We explored the effects of a similar approach in the case of X-ray photosynthesis.

Fig. 8(*a*) shows a TEM micrograph of gold nanoparticles formed after 2-propanol addition (0.6 ml per 40 ml of the precursor solution) and 5 min X-ray exposure. The particle size is 8–15 nm and there is a reasonable distribution. The visible-light absorption spectra of Fig. 8(*b*) show that 2-propanol does not affect the position and the width of the plasmon peak but it does weaken its intensity. These results are different with respect to the extensive data for γ-ray irradiation (Belloni *et al.*, 1998; Gachard *et al.*, 1998; Temgire & Joshi, 2004).

4. Discussions

4.1. X-ray irradiation effects

The most noteworthy discovery of our study is the evolution of the particle structure as a function of the X-ray exposure time, from cross-linking to dispersed individual particles. This evolution sharply differs from other kinds of irradiation and from procedures based on chemical reduction.

When bombarded with high-energy photons, colloidal particles can be damaged and this can lead to photofragmentation, photofusion or other

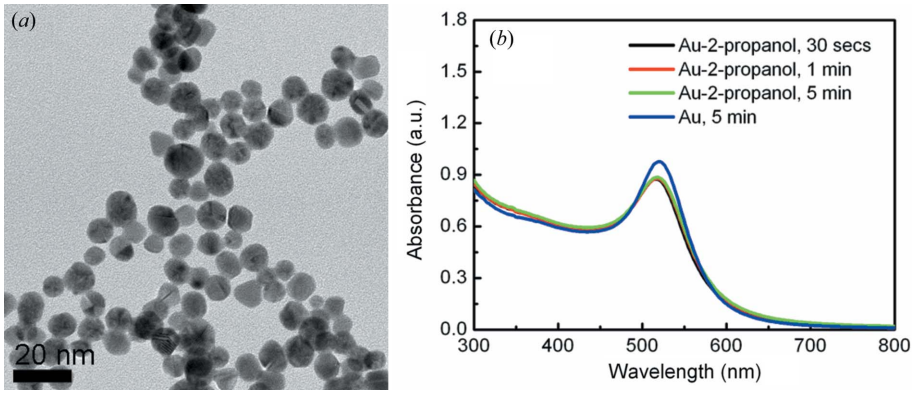

Figure 8
(*a*) TEM micrograph of colloidal gold particles formed in solutions with 2-propanol added, after a 5 min X-ray exposure; (*b*) visible-light absorption spectra of gold nanoparticles formed with different exposure times for a 10 ml precursor solution ([$HAuCl_4$] = 1 m*M*). The amount of 2-propanol was 0.6 ml for each 40 ml of gold precursor solution.

phenomena. The size, shape and morphology of metallic nanoparticles such as gold or silver induced by laser irradiation has been extensively studied (Takami *et al.*, 1996; Kurita *et al.*, 1998; Mohamed *et al.*, 1998; Link *et al.*, 2000; Jin *et al.*, 2001). Takami *et al.* (1996) reported a size reduction of Au particles exposed to laser photons with 532 nm wavelength; Link *et al.* (2000) explained these results in terms of surface melting owing to heating by surface plasmon absorption. Jin *et al.* (2001) described an intriguing shape evolution of Ag particles from nanospheres to nanoprisms induced by 350–700 nm photons. In these photochemical mechanisms the effects depend on the photon energy and are related to the surface plasmon resonance.

The phenomena are quite different for other types of radiation such as γ-rays, X-rays or charged particles (*e.g.* electrons and protons). Each photon or charged particle can ionize a large number of molecules along its track or bring them to different excited states. The products of the corresponding radiochemical reactions are very complicated in terms of energy levels and chemical species (Spinks & Woods, 1976). The mechanisms of X-ray-induced fusion and fragmentation are different from laser ablation owing to the important role of water in the energy absorption. For ultraviolet and visible laser irradiation, water absorption is minimal. For X-ray irradiation, the energy is absorbed both by the particles and by the water; when the solution is diluted as in our case, water absorption prevails.

Since the photon energies of both X-rays and γ-rays are well above the threshold energy for water radiolysis [around 6.6 eV for the photodecomposition of water (Thomsen *et al.*, 1999)], we expect no major differences between the species produced by these types of radiation. Other aspects, however, could be different because of the lower photon energy and much larger flux of X-rays. This point is confirmed by precursor solution temperature measurements. For 10 ml and 5 min X-ray exposure, the average temperature increase was 11 K. Another control measurement involving only de-ionized H_2O (10 g) gave almost the same value. This temperature increase is quite remarkable and the corresponding effects must be taken into account.

Such effects could be responsible for the peculiar morphological transition and photofragmentation after prolonged X-ray irradiation. X-ray photons can, *via* secondary electrons, ionize or excite a large number of water molecules and gold ions along their path. The 'activated' solvent can supply reducing radicals to neighboring gold ions and contribute to the formation of zero-valence gold clusters. These small gold clusters combine to form the initial gold nanoparticles.

Owing to the large X-ray energy absorption, the surface temperature of such nanoparticles can increase above the melting point. This enables the surfaces of close particles to fuse together leading to cross-linking. The resulting gold cluster assemblies diffused from their initial position owing to concentration gradients and heat flow.

After a sufficient exposure time, the inter-connected gold particles completely fill the reaction bath. The absorbed X-ray energy can now lead to fragmentation and to the formation of smaller gold clusters. Owing to the temperature increase of the precursor solution, such small clusters tend to fuse together forming larger clusters as in the case of the annealing-induced fusion of Au nanoparticles (Sutter *et al.*, 2005). After all the cross-linked particles are fragmented, a well dispersed colloidal solution remains.

4.2. Radical scavenger effects

The dissipation of X-ray energy throughout the solvent facilitates the initial homogeneous distribution of the radiolytically produced species, including e^-_{aq}, H^+, $H^\bullet$, $OH^\bullet$, H_2O_2 and H_2. As previously mentioned, we expect the species produced by X-rays to be similar to those yielded by γ-rays. However, the dynamic balance between different reaction mechanisms can be quite different owing to the very high intensity of synchrotron X-rays. The solvated electrons, e^-_{aq} and $H^\bullet$ are strong reducing agents that enable the reduction of metal ions into metallic clusters.

In contrast, the OH radicals cause the re-oxidization of the metal atoms to their ionic state. The overall amount of reduced metallic clusters reflects the interplay of these two opposite actions. In γ-ray synthesis, an OH radical scavenger such as 2-propanol is generally added to the solution to reduce the OH-induced oxidation.

We found, on the contrary, that 2-propanol is not required in the case of synchrotron X-ray irradiation. Rather than having a positive role, the addition of 2-propanol reduces the yield of colloidal gold as revealed by the decreased optical absorption intensity (see Fig. 8*b*).

The cause of this reduction is not clear at present. Note that 2-propanol is a scavenger for both OH and H radicals, these latter being strong reducing agents in radiolysis solutions. We can thus propose that 2-propanol plays a positive role during the initial steps of photoreduction by protecting the Au atoms from re-oxidization. However, once the cross-linked gold colloidals are created, this effect decreases. We are currently analyzing the solution conditions (composition, temperature, pH value, ionic strength *etc.*) that can influence the kinetic conditions for OH and H radical scavenging, which might be quite different from traditional radiolytic reactions as demonstrated by the above-mentioned scavenger effect.

5. Conclusions

We discovered a series of intriguing phenomena affecting the structure of colloidal Au during synchrotron X-ray exposure. As the exposure time increases, the morphology of the formed gold nanoparticles changes from interconnected structures to well dispersed nanosols. These phenomena can be explained by the very high energy rate deposited by the X-ray beam in the precursor solution. We also found that a radical scavenger, although essential in γ-ray photosynthesis, is not required when X-rays replaced the γ-rays.

We thank Y. C. Yang and C. C. Kim for stimulating discussions, and R. S. Liu for his assistance in the experiments. This work is supported by the National Science and Technology Program for Nanoscience and Nanotechnology, the Thematic Research Project of Academia Sinica, the National Synchrotron Radiation Research Center (Taiwan), the Creative Research Initiatives (Functional X-ray Imaging) of MOST/KOSEF, the Center for Biomedical Imaging (CIBM) in Lausanne, partially funded by the Leenaards and Jeantet foundations, the Swiss Fonds National de la Recherche Scientifique and the EPFL.

References

Bae, C. H., Nam, S. H. & Park, S. M. (2002). *Appl. Surf. Sci.* **197–198**, 628–634.
Baik, S., Kim, H. S., Jeong, M. H., Lee, C. S., Je, G. H., Hwu, Y. & Margaritondo, G. (2004). *Rev. Sci. Instrum.* **75**, 4355–4358.
Belloni, J., Mostafavi, M., Remita, H., Marignier, J.-L. & Delcourt, M.-O. (1998). *New J. Chem.* **22**, 1239–1255.
Borse, P. H., Yi, J. M., Je, J. H., Tsai, W. L. & Hwu, Y. (2004). *J. Appl. Phys.* **95**, 1166–1170.
Chah, S. W., Hammond, M. R. & Zare, R. N. (2005). *Chem. Biol.* **12**, 323–328.
Daniel, M. C. & Astruc, D. (2004). *Chem. Rev.* **104**, 293–346.
Fujita, H., Izawa, M. & Yamazaki, H. (1962). *Nature (London)*, **196**, 666–667.
Gachard, E., Remita, H., Khatouri, J., Keita, B., Nadjo, L. & Belloni, J. (1998). *New J. Chem.* **22**, 1257–1265.
Glomm, W. R. (2005). *J. Dispersion Sci. Technol.* **26**, 389–414.
Jin, R. C., Cao, Y. W., Mirkin, C. A., Kelly, K. L., Schatz, G. C. & Zheng, J. G. (2001). *Science*, **294**, 1901–1903.
Karadas, F., Ertas, G., Ozkaraoglu, E. & Suzer, S. (2005). *Langmuir*, **21**, 437–442.
Kreibig, U. & Genzel, L. (1985). *Surf. Sci.* **156**, 678–700.
Kurita, H., Takami, A. & Koda, S. (1998). *Appl. Phys. Lett.* **72**, 789–791.
Lee, H. J., Je, J. H., Hwu, Y. & Tsai, W. L. (2003). *Nucl. Instrum. Methods B*, **199**, 342–347.
Lee, T. M., Oldenburg, A. L., Sitafalwalla, S., Marks, D. L., Luo, W., Toublan, F. J.-J., Suslick, K. S. & Boppart, S. A. (2003). *Opt. Lett.* **28**, 1546–1548.
Link, S., Burda, C., Mohamed, M. B., Nikoobakh, B. & El-Sayed, M. A. (2000). *J. Phys. Chem.* **104**, 6152–6163.
Loo, C., Hirsch, L., Lee, M. H., Chang, E., West, J., Halas, N. & Drezek, R. (2005). *Opt. Lett.* **30**, 1012–1014.
Loo, C., Lowery, A., Halas, N., West, J. & Drezek, R. (2005). *Nano Lett.* **5**, 709–711.
Ma, Q., Moldovan, N., Mancini, D. C. & Rosenberg, R. A. (2000). *Appl. Phys. Lett.* **76**, 2014–2016.
Mohamed, M. B., Ismail, K. Z., Link, S. & El-Sayed, M. A. (1998). *J. Phys. Chem. B*, **102**, 9370–9374.
Mulvaney, P. (2001). *MRS Bull.* **12**, 1009–1013.
O'Neal, D. P., Hirsch, L. R., Halas, N. J., Payne, J. D. & West, J. L. (2004). *Cancer Lett.* **209**, 171–176.
Osawa, M., Hoshino, M., Akita, M. & Wada, T. (2005). *Inorg. Chem.* **44**, 1157–1159.
Rosenberg, R. A., Ma, Q., Lai, B. & Mancini, D. C. (1998). *J. Vac. Sci. Technol. B*, **16**, 3535–3538.
Schmid, G. & Corain, B. (2003). *Eur. J. Inorg. Chem.* pp. 3081–3098.
Siwy, Z., Trofin, L., Kohli, P., Baker, L. A., Trautmann, C. & Martin, C. R. (2005). *J. Am. Chem. Soc.* **127**, 5000–5001.
Spinks, J. W. T. & Woods, R. J. (1976). *Introduction to Radiation Chemistry*, 2nd ed. New York: John Wiley and Sons.
Sun, Q., Wang, Q., Rao, B. K. & Jena, P. (2004). *Phys. Rev. Lett.* **93**, 186803.
Sutter, E., Sutter, P. & Zhu, Y. (2005). *Nano Lett.* **5**, 2092–2096.
Sylvestre, J. P., Poulin, S., Kabashin, A. V., Sacher, E., Meunier, M. & Luong, J. H. T. (2004). *J. Phys. Chem. B*, **108**, 16864–16869.
Takami, A., Yamada, H., Nakano, K. & Koda, S. (1996). *Jpn. J. Appl. Phys.* **35**, L781–L783.
Temgire, M. K. & Joshi, S. S. (2004). *Radiat. Phys. Chem.* **71**, 1039–1044.
Thomsen, C. L., Madsen, D., Keiding, R., Thogersen, J. & Christiansen, O. (1999). *J. Chem. Phys.* **110**, 3453–3462.
Yang, Y. C., Wang, C. H., Hwu, Y. & Je, J. H. (2006). *Mater. Chem. Phys.* **100**, 72–76.
Wang, C. H., Hua, T. E., Chien, C. C., Yu, Y. L., Yang, T. Y., Liu, C. J., Leng, W. H., Hwu, Y., Yang, Y. C., Kim, C. C., Je, J. H., Chen, C. H., Lin, H. M. & Margaritondo, G. (2007). *Mater. Chem. Phys.* doi:10.1016/j.matchemphys.2007.06.024.
Zharov, V. P., Galitovskaya, E. N., Johnson, C. & Kelly, T. (2005). *Lasers Surg. Med.* **37**, 219–226.